21PFL-0574

CFD Modeling of Reacting Diesel Sprays with Primary Reference fuel

Authors:
Qiyan Zhou - Shanghai Jiao Tong University
Tommaso Lucchini and Gianluca D'Errico - Politecnico di Milano
Ricardo Novella and Jose M Garcia-Oliver - Universitat Politècnica de València
Xingcai Lu - Shanghai Jiao Tong University

Abstract

Computational fluid dynamics (CFD) modeling has many potentials for the design and calibration of modern and future engine concepts, including facilitating the exploration of operation conditions and casting light on the involved physical and chemical phenomena. As more attention is paid to the matching of different fuel types and combustion strategies, the use of detailed chemistry in characterizing auto-ignition, flame stabilization processes and the formation of pollutant emissions is becoming critical, yet computationally intensive. Therefore, there is much interest in using tabulated approaches to account for detailed chemistry with an affordable computational cost. In the present work, the tabulated flamelet progress variable approach (TFPV), based on flamelet assumptions, was investigated and validated by simulating constant-volume Diesel combustion with primary reference fuels - binary mixtures of n-heptane and iso-octane. Simulations were initially carried out to evaluate and compare the performance of two kinetic models in homogeneous reactors and laminar diffusion flames, followed by turbulent reacting spray simulations considering different fuels, ambient temperatures, and oxygen concentrations. The sensitivity study of the turbulent Schmidt number was then conducted, and results in terms of ignition delay and lift-off length were compared with experimental data to determine a more appropriate global constant. Finally, parametric variations of ambient temperature and oxygen concentration were performed for six fuel blends ranging from PRF0 (n-heptane) to PRF100 (iso-octane), confirming the validity of the TFPV model.

Introduction

Legislative requirements aimed at promoting energy efficiency, energy security and environmental protection are driving the changes in engine design, which has challenged the efforts of many researchers over the past half-century [1, 2, 3, 4]. From a Diesel engine standpoint, the primary development trend is to reduce soot and NO_x at affordable cost without compromising efficiency [5]. It is best achieved by lowering the reactivity of fuel, e.g. by adding appropriate fuel additives or using gasoline-like fuels, which increases ignition and mixing times, and thereby mitigates emissions typically generated in conventional Diesel engines [6]. Therefore, there is much interest in using gasoline-like fuels in compression ignition engine. However, the implementation of such technology is not very straightforward in practical vehicle engines, since its success demands an enhanced understanding of complex multi-scale physics and chemistry of turbulent spray flames with different fuel types to achieve an intelligent ignition control. This has been at the forefront of engine research, and requires not only experimental efforts in optically accessible rigs [7, 8], but also predictive computational fluid dynamics tools to gain more insight into combustion process and carry out investigations that would prove to be experimentally laborious and expensive [9].

From the combustion modeling point of view, varying from Diesel-like to gasoline-like fuels further emphasizes the use of detailed chemistry and the consideration of different combustion modes. In particular, the models must be able to capture subtle influences of fuel composition on efficiency and emissions and must be able to deal with mixed-mode turbulent combustion (from kinetically controlled to turbulent-mixing controlled to premixed flame propagation) [10]. As to the first point, we can mention the use of tabulated kinetics, including realistic chemistry by means of pre-tabulated solutions based on assumed flame structures [11, 12, 13, 14]. This method assumes that thermo-chemical evolution in the composition and temperature spaces can be parameterized by a reduced set of variables [15]. Techniques that fall into this category include the flame-generated manifold (FGM) [16], the flame prolongation of ILDM (FPI) [17] or the flamelet progress variable (FPV) [18]. Among them, one interesting approach, the tabulated flamelet progress variable (TFPV) based on approximated diffusion flamelets [19, 20, 21], has been comprehensively validated in the modeling of spray flames with single and double injections [22, 23], as well as light- and heavy-duty Diesel engines [24, 25]. The successful application of the TFPV approach in the presence of multiple injections shows that it should potentially be able to capture lean-rich premixed and diffusion flames as well as auto-ignition modes of combustion, simultaneously [26].

Obtaining accurate temporally and spatially resolved data of key scalars and velocity in turbulent spray flames is essential for CFD simulations. In the Reynolds-Averaged Navier-Stokes (RANS) framework, which is the most often used in the design of practical IC engines, turbulent flow generally assumes the gradient diffusion hypotheses to close the scalar-flux term, and thus requires a model constant to correlate the turbulent mass diffusivity to the turbulent viscosity, known as turbulent Schmidt number Sc_t [27]. Dating back to Spalding [28], a turbulent Schmidt number of $Sc_t = 0.7$ was used, giving a good agreement with experimental data. On the other hand, Launder [29] pointed out Sc_t showed the value of 0.9 for turbulence near the wall. Quoting from these results, the values of 0.7 or 0.9 have

been used for most of the CFD studies and set as default in most CFD software [30]. However, the optimum values of Sc_t used by various researchers are widely spread from 0.1 to 2.2 [31], alluding to the fact that prescribing a global value is problem-dependent. For instance, Mompean [32] found a value of $Sc_t = 0.4$ appropriate while Crocker et al. [33] used a value as low as 0.25 for their simulations of a gas turbine combustor. It is confirmed that the value of Sc_t has a significant effect on the prediction of mass or fuel diffusion and the consequent combustion process. Eklund et al. [34] observed that an assumption of low Sc_t value can lead to unstart in the scramjet engine, whereas high one can lead to flame blowout. Regarding turbulent spray flames, the choice of Sc_t value is of paramount importance, since combustion is mainly governed by the mixing of fuel and oxidizer, being inversely proportional to the turbulent Schmidt number [35]. For this reason, a sensitivity study of ignition and flame stabilization to the turbulent Schmidt number is performed in this work, to determine the optimum value of Sc_t and ensure high confidence in the following Diesel spray modeling.

The purpose of this study is to extensively assess the potentialities and limits of the TFPV model in simulating Diesel-type sprays with n-heptane, iso-octane and four intermediate blends known as primary reference fuels (PRF), representing the transition from conventional Diesel-like fuel (n-heptane) to a gasoline-like one (iso-octane) in terms of ignition behavior. Non-reacting spray in a high-pressure high-temperature vessel using the specifications from the Engine Combustion Network (ECN) [36] was first simulated to validate the accuracy of the computational setups. Parametric variations of fuel content, injection pressure, ambient temperature, and oxygen concentration were considered in the transient high-pressure spray flames calculations. The computed ignition delays (ID) and lift-off lengths (LOL) were compared with experiments [37, 38], evaluating the performance of different chemistry mechanisms and global values of the turbulent Schmidt number. Following these sensitivity studies and the determination of more favored numerical methodology, the comprehensive validation of the TFPV approach was conducted by performing the parametric variations of ambient temperature and oxygen content for each fuel blend.

Combustion model

The main purpose of the TFPV model is to provide a realistic description of the turbulent diffusion flames with an affordable computational cost. Owing to the use of progress variable and scalar dissipation rate, it takes into account turbulence-chemistry interaction, sub-grid mixing, premixed flame propagation, and gives correct predictions of extinction, re-ignition and flame stabilization processes. The operation of the TFPV model is generally divided into two parts: generating the offline TFPV table and coupling it with the CFD solver.

TFPV table

For generating the TFPV table, first, a set of constant pressure, auto-ignition processes should be calculated and the resultant chemistry information needs to be tabulated into a Homogeneous Reactor (HR) chemistry table. The operation of such approach is illustrated in Figure 1. A chemical mechanism needs to be specified for the HR calculations, as well as a range of initial conditions including mixture fraction Z, pressure p, temperature T_u, and initial compositions. To include the effect of fuel evaporation in spray combustion cases, the initial reactor temperature can be expressed as a function of the user-provided oxidizer temperature $(T_{Z=0})$, fuel temperature $(T_{Z=1})$ and heat of evaporation:

$$h(Z) = (1 - Z) \cdot h(T_{Z=0}) + Z \cdot h(T_{Z=1}) - Z \cdot h_l(T_{Z=1}) \quad (1)$$

$$T_u(Z) = T(h(Z)) \quad (2)$$

For any specified condition, the following equation is solved for all chemical species:

$$\frac{\mathrm{d}Y_i}{\mathrm{d}t} = \dot{\omega}_i(T, p, Y_i, \cdots, Y_{N_s}) \quad (3)$$

with the reactor temperature T computed directly from the initial enthalpy value. After each time step, the evaluation of progress variable C together with the computation of chemical compositions using the *virtual species* approach [39, 40] are performed. The definition of combustion progress variable proposed by Lehtiniemi et al. [41] was adopted in the present work, known as h_{298}, which is calculated as the difference between the current and initial value of the reactor formation enthalpy:

$$C = \sum_{i=1}^{N_s} h_{298,i} \cdot Y_i(t) - \sum_{i=1}^{N_s} h_{298,i} \cdot Y_i(0) \quad (4)$$

where C equals to the heat released due to combustion, characterizing each point in the thermochemical state space and being appropriate for a transport equation. N_s represents the total number of chemical species involved in the specified mechanism. After each reactor calculation, the progress variable is normalized:

$$c = \frac{C - C_{min}}{C_{max} - C_{min}} \quad (5)$$

where C_{min} and C_{max} represent the minimum and maximum values of the progress variable at initial and after auto-ignition states, which are stored in the table as a function of Z, T_u, P. Progress variable reaction rates, computed from the values of times at which the specified c_i values are found, with the forward differencing scheme as shown in Equation 6, are stored as a function of the discrete values of c, together with chemical compositions. Instead of the entire set of species, only seven virtual species (N_2, O_2 $fuel$, CO_2, CO, H_2O, H_2) are tabulated to avoid excessive memory consumption. Their mass fractions are computed to preserve the main thermochemical properties of the full set of species involved in the specified mechanism [39, 40]. In addition, the mass fraction of chemical species which are of interest to the user (Y_o in Figure 1) are also included in the table, either for post-processing reason or because they have to be used by the related sub-models for describing the formation of main pollutants.

$$\dot{c}_i = \frac{c_{i+1} - c_i}{t_{i+1} - t_i} \quad (6)$$

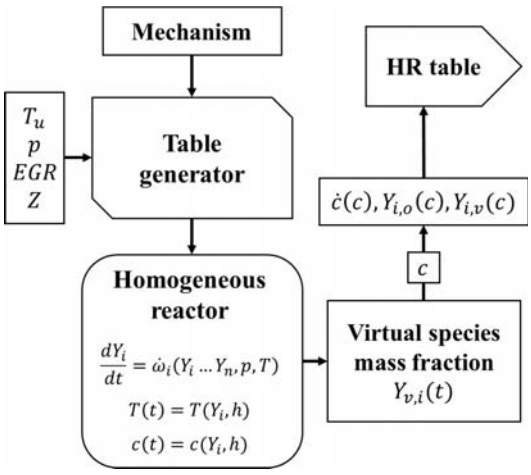

Figure 1: Generation of chemistry table based on homogeneous reactor assumption.

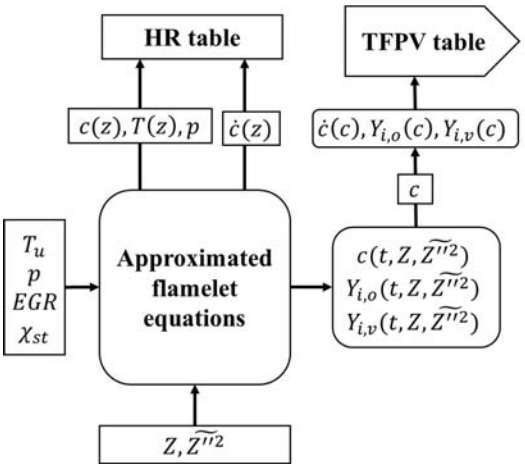

Figure 2: Generation of TFPV chemistry table.

Figure 2 summarizes the generation of the TFPV table. A range of unburned temperature, pressure, stoichiometric scalar dissipation rate, mixture fraction and its variance are provided for the unsteady diffusion flame calculations by means of solving the approximated flamelet equations in the mixture fraction space [41, 20, 21]. On the basis of unity Lewis number assumption [42], the flamelet equations can be formulated as:

$$\rho\frac{\partial C}{\partial t} = \rho\frac{\chi_z}{2}\frac{\partial^2 C}{\partial Z^2} + \dot{C} \tag{7}$$

$$\rho\frac{\partial h}{\partial t} = \rho\frac{\chi_z}{2}\frac{\partial^2 h}{\partial Z^2} + \frac{\partial p}{\partial t} \tag{8}$$

where the progress variable source term $\dot{C}$ is calculated as $\dot{c}$ taken from the HR chemistry table multiplied by the term $C_{max} - C_{min}$. It is set to zero when equivalence ratio $\phi > 3$ to avoid too anticipated ignitions due to progress variable diffusion. The function form of the dependence of scalar dissipation rate χ_z on mixture fraction Z in the flamelet is typically represented by an error function profile [43]:

$$\chi = \chi_{st}\frac{exp(-2\left|erfc^{-1}(2Z)\right|^2)}{exp(-2\left|erfc^{-1}(2Z_{st})\right|^2)} \tag{9}$$

At each time step, the chemical compositions in terms of the virtual species $Y_{i,v}(Z,t)$, and the progress variable $C(Z,t)$ can be estimated for the prescribed values of Z. The mixture fraction variance $\widetilde{Z''^2}$ is computed from the user-specified mixture fraction segregation factors:

$$S_Z = \frac{\widetilde{Z''^2}}{Z(1-Z)} \tag{10}$$

The flamelet calculations results are then processed to account for sub-grid mixing by virtue of assuming the β-PDF distribution for both progress variable and chemical compositions:

$$Y_i(Z, \widetilde{Z''^2}) = \int_0^1 Y(Z)\beta(Z, \widetilde{Z''^2})\mathrm{d}Z \tag{11}$$

$$C(Z, \widetilde{Z''^2}) = \int_0^1 C(Z)\beta(Z, \widetilde{Z''^2})\mathrm{d}Z \tag{12}$$

At the end of any diffusion flame calculation, for all values of Z and $\widetilde{Z''^2}$, the progress variable is normalized, and its reaction rate is estimated according to Equations 5-6. Computed data are then interpolated for the discrete values of progress variable to generate the chemistry table.

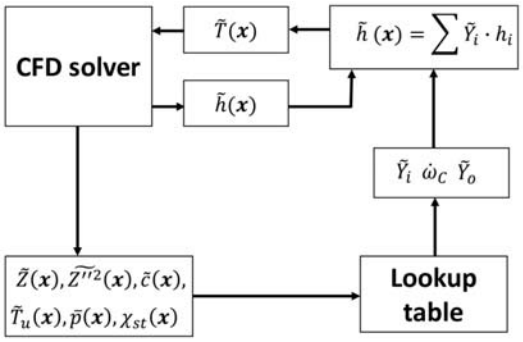

Figure 3: Operation of combustion models based on tabulated kinetics.

CFD solver

Figure 3 presents the operation principle of the TFPV combustion model, illustrating the mutual interaction between CFD solver and lookup table. In the CFD domain, additional transport equations need to be solved for mixture fraction Z, mixture fraction variance $\widetilde{Z''^2}$, progress variable C, unburned gas enthalpy h_u, and stoichiometric scalar dissipation rate χ_{st}. In this work, the following equation is solved for mixture fraction, accounting for the spray evaporation effects:

$$\frac{\partial\overline{\rho}\widetilde{Z}}{\partial t} + \nabla(\rho\widetilde{U}\widetilde{Z}) - \nabla(\frac{\widetilde{\mu}_t}{Sc_t}\nabla\widetilde{Z}) = \dot{S}_Z \tag{13}$$

Assuming the sub-grid distribution of mixture fraction can be represented by the β-PDF, its variance equation needs to be solved:

$$\frac{\overline{\rho}\widetilde{Z''^2}}{\partial t} + \nabla(\overline{\rho}\widetilde{U}\widetilde{Z''^2}) - \nabla(\frac{\widetilde{\mu}_t}{Sc_{\widetilde{Z''^2}}}\nabla\widetilde{Z''^2}) = 2\frac{\widetilde{\mu}_t}{Sc_{\widetilde{Z''^2}}}\left|\nabla\widetilde{Z}\right|^2 - \overline{\rho}\widetilde{\chi} \tag{14}$$

The sink term appearing in Equation 14 is the average scalar dissipation rate, which is a function of turbulent time scale and mixture fraction variance:

$$\widetilde{\chi} = C_\chi\frac{\widetilde{\varepsilon}}{k}\widetilde{Z''^2} \tag{15}$$

The source term in the progress variable transport equation (Equation 16) is taken from the lookup table:

$$\frac{\partial\overline{\rho}\widetilde{C}}{\partial t} + \nabla(\overline{\rho}\widetilde{U}\widetilde{C}) - \nabla(\frac{\widetilde{\mu}_t}{Sc_t}\nabla\widetilde{C}) = \overline{\rho}\dot{C} \tag{16}$$

To consistently access the table data, it is of necessity to solve the transport equation for unburned gas enthalpy h_u which is then used to estimate the unburned gas temperature T_u, being one of the independent variables of the table:

$$\frac{\partial\overline{\rho}\widetilde{h_u}}{\partial t} + \nabla(\overline{\rho}\widetilde{U}\widetilde{h_u}) - \nabla(\widetilde{\alpha_t}\nabla\widetilde{h_u}) = \dot{Q}_s + \frac{\overline{\rho}}{\overline{\rho_u}}\cdot\frac{D\overline{p}}{Dt} \tag{17}$$

where α_t is the turbulent thermal diffusivity and ρ_u is the density of unburned gases which is computed from local cell pressure, chemical compositions at $C = 0$ and T_u. $\dot{Q}_s$ is the source term related to spray evaporation. In each cell, the stoichiometric scalar dissipation rate χ_{st} is computed based on the Hellstrom formulation [42]:

$$\chi_{st} = \frac{\chi}{\int_0^1 \frac{f_{erfc}(Z)}{f_{erfc}(Z_{st})}\tilde{P}(Z)dZ} \tag{18}$$

where f_{erfc} has an erfc-profile and $\tilde{P}(Z)$ is a β-PDF function, whose parameters depend on the mixture fraction and its variance. The local

cell values of Z, $\widetilde{Z''^2}$, C, p, T_u and χ_{st} are then used to access the lookup table, which provides the chemical compositions and the progress variable reaction rate to the CFD solver by performing an inverse, distance weighted interpolation. It should also be highlighted that progress variable diffused from the cool flame could ignite rich mixtures ($\phi > 3$) instantaneously, and high values of C will be diffused back to lean or stoichiometric mixtures resulting in a very anticipated auto-ignition. To avoid this, reaction rates are set to zero in the regions where two-stage ignition does not happen (approximately to $\phi > 3$), which is similar to the flamelet calculations as discussed before (Equations 7).

Computational setup

Numerical simulations were conducted using the Lib-ICE code, a set of solvers and libraries for IC engine simulations developed under the OpenFOAM technology [44, 45, 46]. The standard $k - \varepsilon$ model in the framework of RANS formulation was used for turbulence with the so-called *round jet correction* to predict the penetration of fuel vapor jet [47]. The PISO algorithm was used to couple pressure and velocity equations, ensuring the accuracy in transient flow problems [48]. The evolution of spray is described by a discrete number of computational parcels, each one representing droplets with the same properties. Parcels evolve into the CFD domain in a Lagrangian fashion, exchanging mass, momentum, and energy with the Eulerian gas phase. Specific sub-models are essential to mimic fuel atomization, breakup, heat transfer, evaporation, collision, and wall impingement. In the present work, droplet parcels were generated using a Rosin-Rammler probability density function, followed by activating the Reitz-Diwakar model [49, 50], which reduces the second breakup to a continuous decrease in droplet radius. Droplet evaporation was computed from the droplet size and Spalding mass number while the Ranz-Marshall correlation was used to model heat transfer between the liquid and the surrounding gas phase. Collision and coalescence were neglected since they have a minimum influence on evaporating spray simulations [51, 52]. A 3D mesh was used to represent the entire domain of the combustion vessel, and its cross section is shown in Figure 4, where the red arrow depicts the injection direction. The total number of mesh cells is approximately 0.4 million with optimal cell sizes of 0.2 mm in the vicinity of the nozzle. The mesh structure is similar to what is generally employed in practical IC engine simulations [40, 53]: the grid is refined near the injector and its resolution progressively decreases when moving downstream of the injector and the combustion vessel walls to save the computational time. The oxidation of PRFs was modeled using two reduced mechanisms involving the low-temperature chemistry: the POLIMI kinetic mechanism proposed by Frassoldati et al. [54, 55, 56], consisting of 156 species and 3370 reactions; the LLNL kinetic mechanism developed by Mehl et al.[57], containing 679 species and 5935 reactions. The validation of the POLIMI mechanism was performed in [54], considering the predictions of ignition delay times for stoichiometric fuel/air mixture of a gasoline surrogate (ternary mixture of iso-octane, n-heptane and toluene) at 15 and 50 bar, as well as the laminar flame speeds for neat iso-octane, n-heptane, toluene and a ternary mixture at 298 and 358 K. Regarding the LLNL mechanism, the predictions of stoichiometric oxidation of pure components (iso-octane, n-heptane, toluene, 1-hexene), binary and ternary mixtures were validated with experimental data in rapid compression machine, shock tube and jet stirred reactor covering a wide range of conditions pertinent to practical IC engines (3-50 bar, 650-1200 K) [57]. For each kinetic scheme, 16 chemistry tables were generated, one for each fuel and oxygen concentration. Details of the table discretization is reported in Table 1, representing a good compromise between accuracy and computational costs. A 700-1000 K temperature range and three pressure levels were considered to cover all the analyzed ambient thermodynamic conditions given in Table 2. 33 points were used to discrete the mixture fraction space and seven stoichiometric scalar dissipation rates were chosen, following a logarithmic curve.

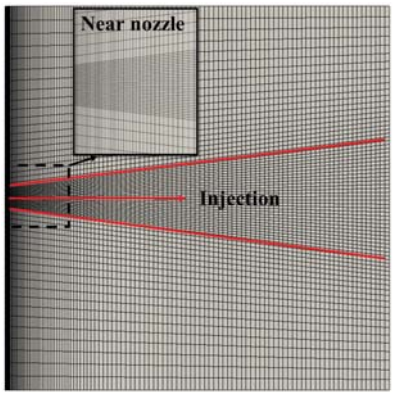

Figure 4: Cross-section of the computational domain.

Table 1: Chemistry table discretization.

Temperature [K]	700, 750, 800, 850, 900, 950, 1000
Pressure [bar]	50, 60, 70
Equivalence ratio	0, 0.1, 0.2, 0.4, 0.5, 0.6, 0.7, 0.75, 0.8, 0.85, 0.9, 0.95, 1, 1.05, 1.1, 1.15, 1.2, 1.25, 1.3, 1.35, 1.4, 1.5, 1.6, 1.7, 1.8, 1.9, 2, 2.2, 2.4, 2.6, 2.8, 3, 1e15
mixture fraction segregation	0, 0.001, 0.005, 0.01, 0.05, 0.1, 1
Scalar dissipation rate χ_{st} [s^{-1}]	0, 1, 3, 7, 20, 55, 100

Results and discussion

Experiments conducted in the CMT combustion vessel, where the Diesel-like conditions (high temperature and high pressure) can be reached and optical techniques including high-speed Schlieren and time-averaged OH^* chemiluminescence are available [8, 58, 38], were used for the validation and assessment of the TFPV approach. The Spray A injector within the Engine Combustion Network (ECN) [36], an international collaboration among different research laboratories, was used, which has a single-hole nozzle with a nominal diameter of 0.09 mm (# 210675). Injection duration was kept at 3.5 ms and ambient density was maintained at 22.8 kg/m^3. Table 2 reports the simulated reacting conditions: six blends of n-heptane and iso-octane in increments of 20% were tested, as well as the parametric variations of ambient temperature, oxygen mole fraction, and injection pressure. In Table 2, the nomenclature of each blend is PRF#, where the # stands for PRF number, the mass fraction of iso-octane. Additionally, an inert case under the baseline Spray A condition (T = 900 K, ρ_{amb} = 22.8 kg/m^3) was also simulated for PRF0 to assess if the choice of mesh size and spray sub-models can correctly describe the liquid and vapor distribution, which is a fundamental prerequisite for any reacting spray simulation. The computed vapor penetration is compared with the measured data in Figure 5 (a), evidencing a rather good agreement with experiments. The computed liquid penetration is obtained in two different ways: 1. the mass-based approach, defining the liquid length as the distance from injector where 99% injected mass is reached; 2. the projected liquid volume (PLV) approach [59, 60], which generates a Eulerian liquid volume fraction field from the projection of Lagrangian liquid spray, and defines the liquid penetration using threshold values of 2e-6 and 2e-7. Results from

Table 2: Simulated reacting conditions.

Test	Fuel	O_2 [%]	T_{amb} [K]	P_{inj} [MPa]
1	PRF0	15	900	150
2	PRF0	18	900	150
3	PRF0	21	900	150
4	PRF0	15	800	150
5	PRF0	15	1000	150
6	PRF0	15	900	100
7	PRF0	15	900	50
8	PRF20	15	900	150
9	PRF20	15	800	150
10	PRF20	15	950	150
11	PRF20	18	900	150
12	PRF20	21	900	150
13	PRF40	15	900	150
14	PRF40	15	800	150
15	PRF40	15	950	150
16	PRF40	18	900	150
17	PRF40	21	900	150
18	PRF60	15	900	150
19	PRF60	15	800	150
20	PRF60	15	950	150
21	PRF60	18	900	150
22	PRF60	21	900	150
23	PRF80	15	900	150
24	PRF80	15	800	150
25	PRF80	15	950	150
26	PRF80	18	900	150
27	PRF80	21	900	150
28	PRF100	21	900	150

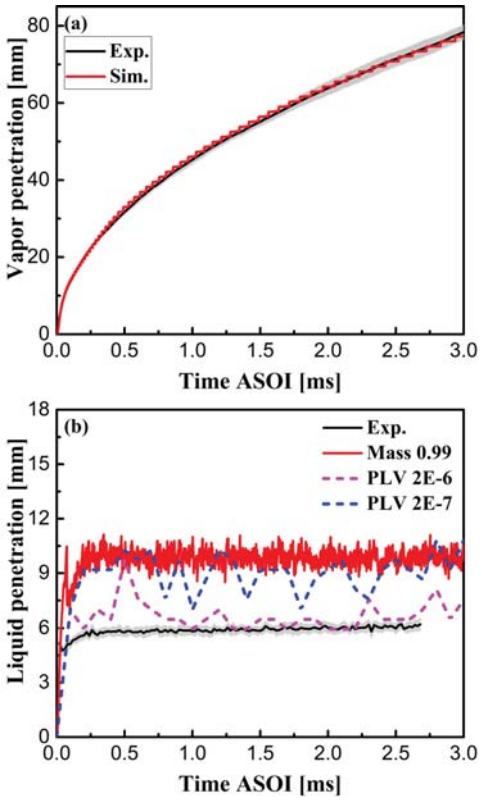

Figure 5: Measured and computed (a) vapor and (b) liquid penetration for the non-reacting baseline case.

these methods are reported in Figure 5, together with experimental data, showing the value from the PLV approach with a threshold value of 2e-6 is very close to the measurement. Such achieved accuracy is adequate for proceeding to combustion simulations and further validation of the numerical setup was reported in [23].

Sensitivity study of chemistry mechanism

Focusing on the evaluation of POLIMI and LLNL kinetic mechanisms, the discussion in this section follows the operation sequence of the TFPV model in order to establish a clear understanding of how chemical schemes interact with combustion in homogeneous reactors, laminar flames and reacting sprays. In this way, the mechanisms are initially assessed in terms of the prediction of cool-flame and high-temperature ignition delays in homogeneous reactors, which are defined as the time spent to reach the initial temperature plus 30 and 400 K [61] and referred as CFID and ID, respectively. Note that all the initial reactor conditions are derived from the corresponding combustion vessel ambient in Table 2 and the adiabatic mixing line formulation (Equation 1). The computed CFID and ID from the two analyzed mechanisms are plotted as a function of Z in Figure 6 for different fuels (PRF0, PRF40, and PRF80). Z_{max} ($\phi = 3$) where the reaction rate was set to zero in all TFPV simulations is shown in black solid line, together with the stoichiometric mixture fraction Z_{st}. Three features of the two-stage ignition are clearly depicted:

1. High-temperature ignition: the LLNL mechanism computes a generally lower ID compared to the POLIMI one, while the shortest ID is identical as well as its corresponding mixture fraction, known as the most reactive mixture fraction Z_{MR} [62], which is of great interest in turbulent non-premixed combustion, as high-temperature ignition happens somewhere along the Z_{MR} isoline, and in particular where the mixture fraction gradients, quantified through the scalar dissipation, are low [63];
2. Cool-flame ignition: a shorter CFID is obtained using the POLIMI mechanism within lean and moderately rich ranges, while an opposite behavior takes place when moving to very rich conditions. Notably, both mechanisms predict that the CFID increases with mixture fraction as well as its slope, indicating a faster cool-flame ignition occurs in lean mixtures, which is probably due to their high initial temperatures. This has been used to argue the initiation of turbulent spray ignition in [64, 65, 61], saying low-temperature reactions often start with lean mixtures in the radial spray periphery, which, in combination with the intense scalar dissipation, initiates a cool flame wave, transporting radicals and heat to the richer core region of the spray head and increasing their reactivity;
3. Cool flame period (the time elapsed between CFID and ID): the LLNL mechanism predicts a shorter cool-flame period, and for both mechanisms, it is also possible to see the convergence of ID and CFID curves, indicating the reduction of this duration when enriching the mixture. This is expected to displace the combustion from lean mixtures to rich ones [64, 65], and favor the high-temperature ignition of rich mixtures [61].

It is worth mentioning that the discussions and descriptions for Figure 6 could be qualitatively applied to the other ambient conditions presented in Figure 7, except the 800-K case (Figure 7 (a)), representing a low-temperature combustion regime for modern engines. Looking at Figure 7 (a), which displays the computed ignition delays for the 800-K ambient, it is possible to see that the POLIMI mechanism ignites slower and predicts relatively higher CFID and ID compared to the LLNL scheme, within the entire mixture fraction spectrum.

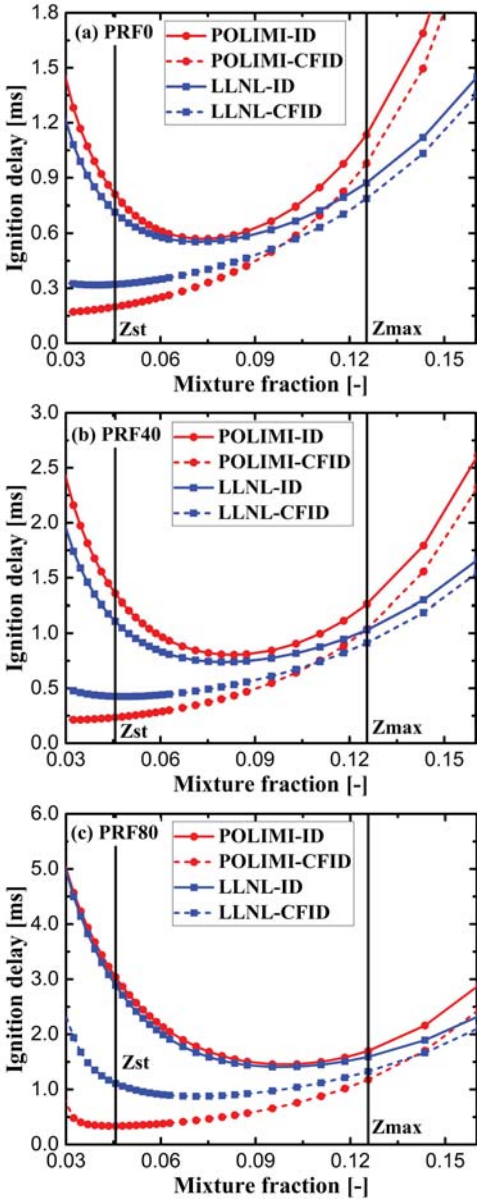

Figure 6: High-temperature and cool-flame ignition delays from homogeneous reactor calculations for (a) PRF0; (b) PRF40 and (c) PRF80. The initial temperatures are derived from adiabatic mixing line for the baseline condition (T_{amb} = 900 K, O_2 = 15%). Mixture fractions corresponding to $\phi = 1$ and $\phi = 3$ are shown in black solid lines and labeled as Z_{st} and Z_{max}, respectively.

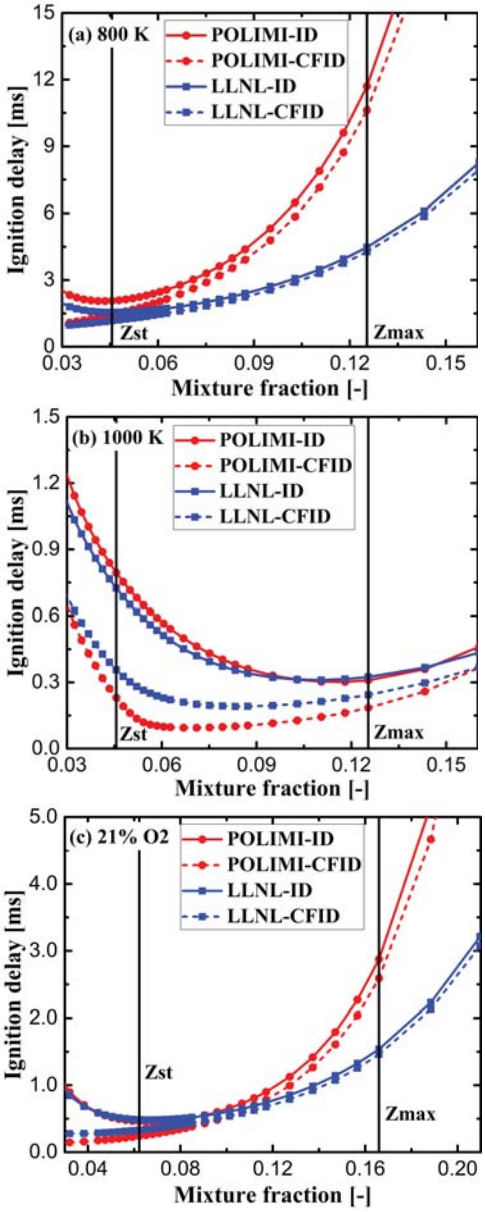

Figure 7: High-temperature and cool-flame ignition delays from homogeneous reactor calculations for PRF0 at (a) T_{amb} = 800 K; (b) T_{amb} = 1000 K and (c) O_2 = 21%. The initial temperatures are derived from adiabatic mixing line for each tested ambient condition. Mixture fractions corresponding to $\phi = 1$ and $\phi = 3$ are shown in black solid lines and labeled as Z_{st} and Z_{max}, respectively.

Moving the discussion and analysis along the performance of the TFPV model, results from homogeneous reactors are mapped into the Z-C space as shown in Figure 8 and Figure 9, where the progress variable reaction rate is visualized in a logarithmic scale. Z_{st} and Z_{max} are represented in white solid lines. Two-stage ignition characteristics can be identified by reaction intensities in different zones, proving the chosen progress variable can trace accurately the low- and high-temperature ignitions:

1. Cool-flame ignition, the region with low progress variable and moderately intense reaction rate, being enhanced as the mixture becomes rich;
2. Cool flame period, the narrow interval between cool-flame and high-temperature ignition, appearing a reduction of reaction rate;
3. High-temperature ignition, corresponds to a substantial increase of progress variable reaction rate. The most intensive reaction can be observed near the stoichiometric or slightly rich mixtures.

Regarding the performance of two kinetic mechanisms, it is important to underline that they perform similarly for the parametric variations of fuel composition, ambient temperature, and oxygen content, while the major difference lies in that the LLNL scheme predicts more intense progress variable reaction rate in cool flame and narrower cool flame period. For the sake of completeness, some observations on the effects of parametric variables are also described:

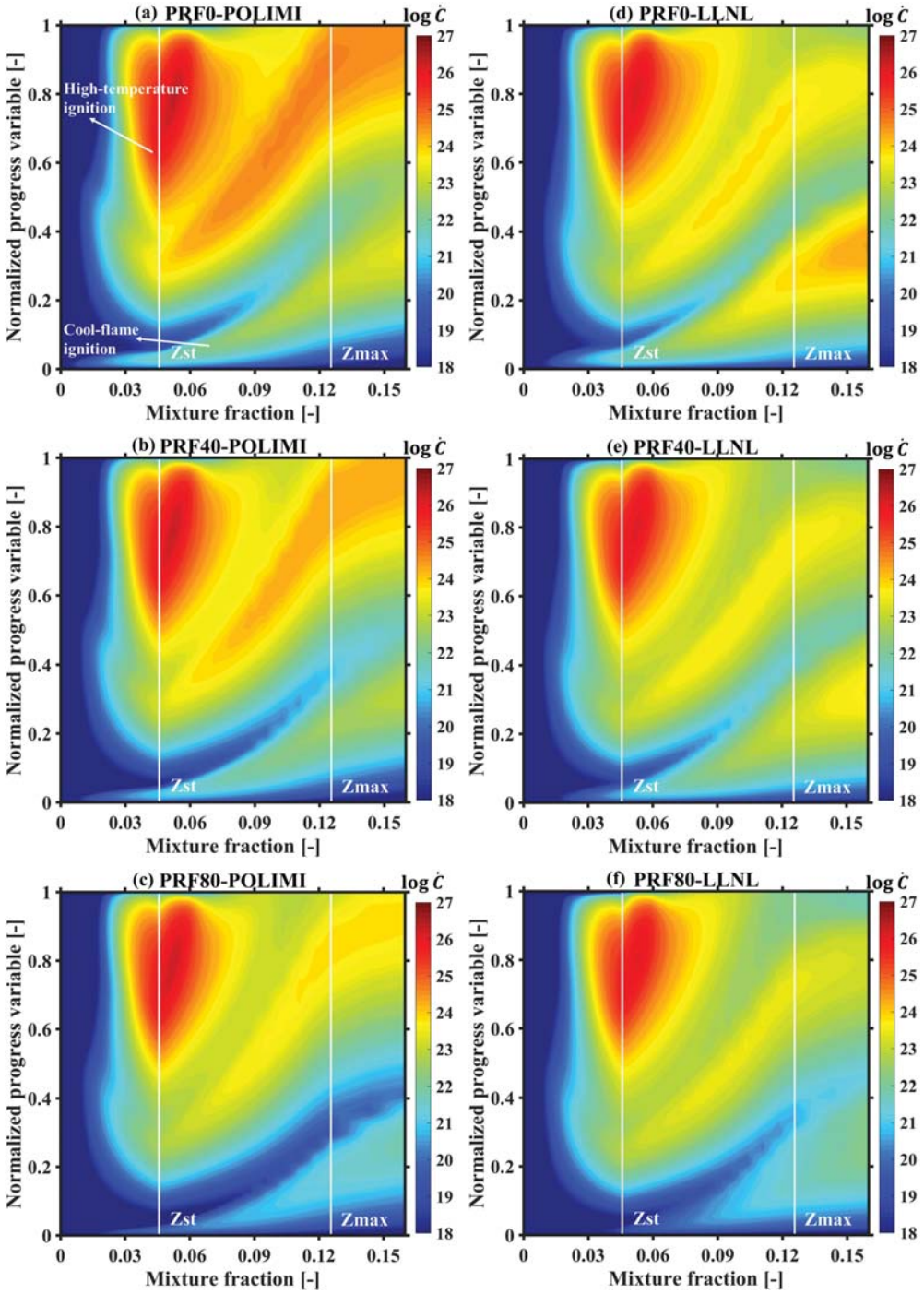

Figure 8: Progress variable reaction rate from homogeneous reactors calculations for different fuels at baseline condition using the POLIMI mechanism: (a) PRF0; (b) PRF40; (c) PRF80 and the LLNL mechanism: (d) PRF0; (e) PRF40; (f) PRF80. The maps are shown in logarithmic scales. White solid lines marked as Z_{st} and Z_{max} represent $\phi = 1$ and $\phi = 3$, respectively.

1. Fuel content (Figure 8(a), (b) and (c)): the role of increasing PRF (RON) number in ignition control is to reduce the chemical reactivity across the whole map, especially in the cool flame zone, and to prolong the cool flame period (wider interval), with a consequent retarded first- and second-stage ignitions;
2. Ambient temperature (Figure 9(a), (b) and Figure 8(a)): the increase of temperature could enhance the chemical reactivity and move the cool-flame ignition in the rich mixtures to very low progress variable, being comparable to the lean ones. Returning to Figure 7(b), marginal difference of the CFID can be seen when varying mixture fraction from 0.06 to 0.125, corresponding to the lean limit of cool flame and Z_{max}, as depicted in Figure 9(b). This might question whether the ignition mechanism of turbulent spray derived from 900-K

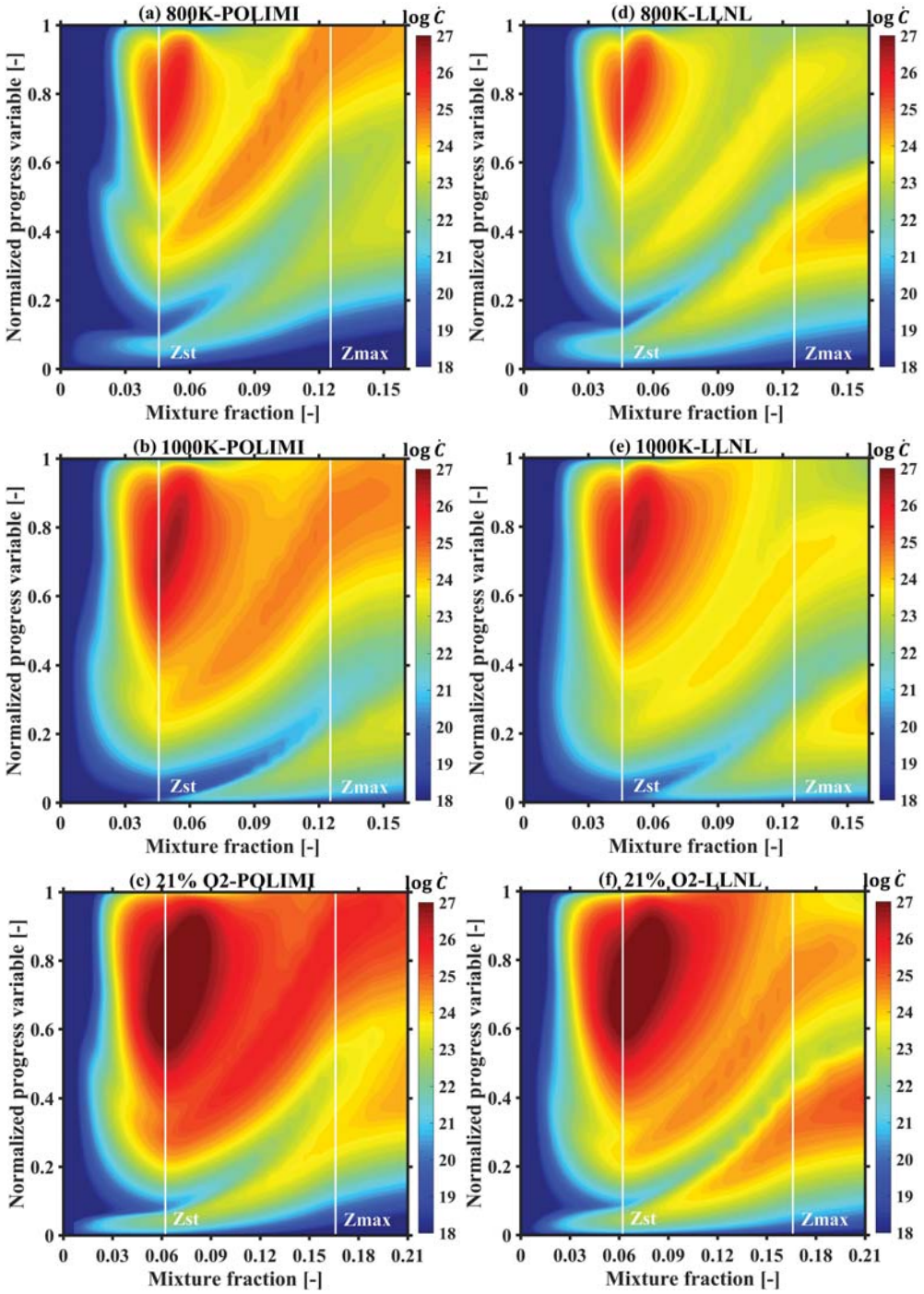

Figure 9: Progress variable reaction rates of PRF0 from homogeneous reactors calculations for different ambient conditions using the POLIMI mechanism: (a) T = 800 K; (b) T = 1000 K; (c) O_2 = 21% and the LLNL mechanism: (d) T = 800 K; (e) T = 1000 K; (f) O_2 = 21%. The maps are shown in logarithmic scales. White solid lines marked as Z_{st} and Z_{max} represent $\phi = 1$ and $\phi = 3$, respectively.

ambient, emphasizing the transport of cool flame products and heat from lean to rich mixtures [64][65][61], can be applied to higher temperatures, where the cool-flame ignition might take place within a range of rich mixtures almost simultaneously;

3. Oxygen concentration (Figure 9(c) and Figure 8(a)): substantial effects of increasing oxygen concentration are observed, including the drastically enhanced reactivity and broadened flammability limits.

As the next step, unsteady laminar diffusion flame calculations were conducted for a stoichiometric scalar dissipation rate value of χ_{st} = 3 s^{-1}. As clearly described in Figure 10 (a), where the flamelet solutions from the POLIMI and LLNL mechanisms are compared for PRF0 at the baseline condition, the first-stage ignition in laminar

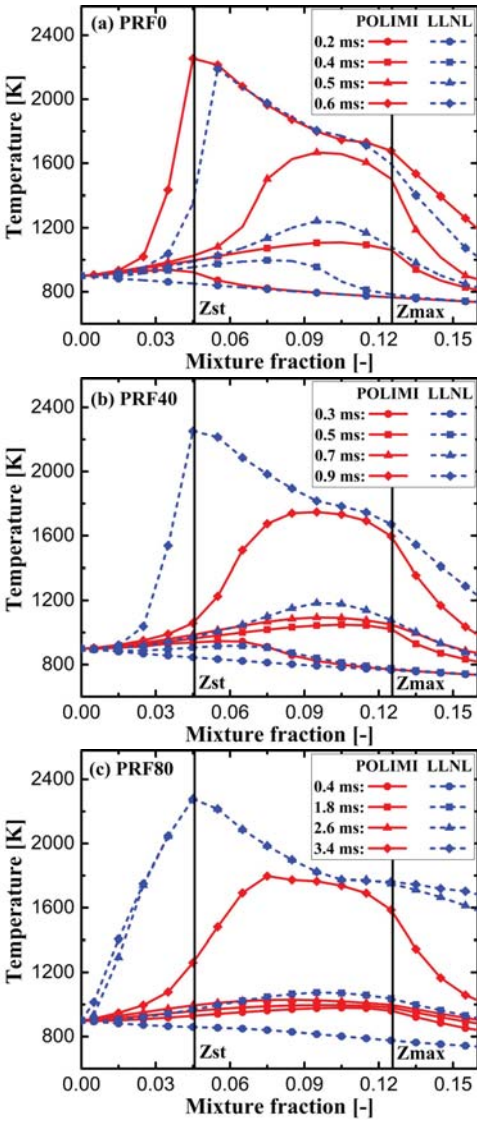

Figure 10: Laminar flames for (a) PRF0 at t = 0.2, 0.4, 0.5, 0.6 ms instants; (b) PRF40 at t = 0.3, 0.5, 0.7, 0.9 ms instants and (c) PRF80 at t = 0.4, 1.8, 2.6, 3.4 ms instants in $Z-T$ space under T_{amb} = 900 K and χ_{st} = 3 s^{-1} condition. Mixture fractions corresponding to $\phi = 1$ and $\phi = 3$ are shown in black solid lines and labeled as Z_{st} and Z_{max}, respectively.

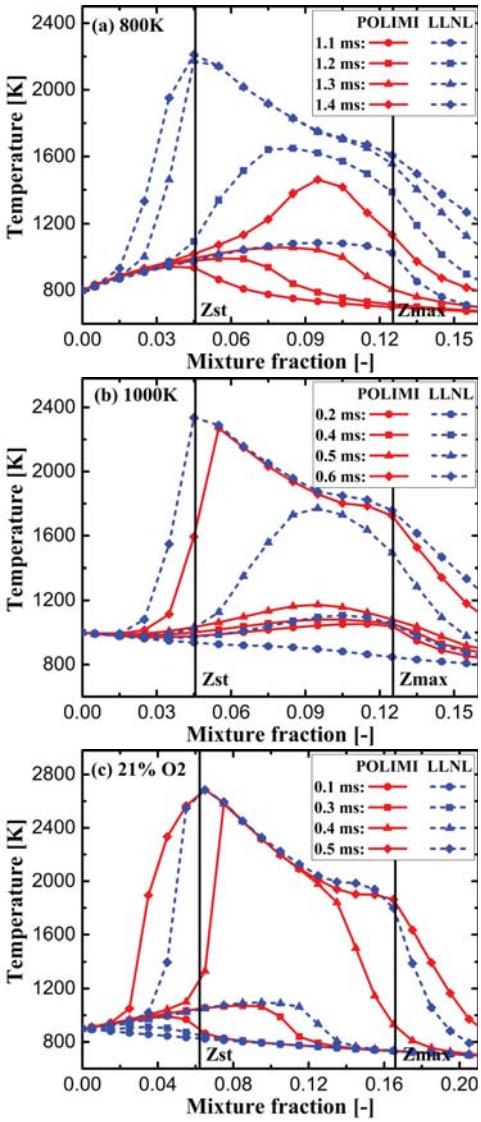

Figure 11: Laminar flames of PRF0 in $Z-T$ space for (a) T = 800 K condition at t = 1.1, 1.2, 1.3, 1.4 ms instants; (b) T = 1000 K condition at t = 0.2, 0.3, 0.4, 0.5 ms instants and (c) O_2 =21% condition at t = 0.1, 0.3, 0.4, 0.5 ms instants with χ_{st} = 3 s^{-1}. Mixture fractions corresponding to $\phi = 1$ and $\phi = 3$ are shown in black solid lines and labeled as Z_{st} and Z_{max}, respectively.

flame starts at the lean mixtures due to their higher initial temperatures and the consequent shortest CFID as discussed in Figure 6(a), followed by a combustion displacement to richer mixtures and high-temperature ignition initialized around Z_{MR}. Note that the value of Z_{MR} in laminar flame (circa 0.1) is slightly higher than the one in homogeneous reactor (circa 0.075), demonstrating its mild dependence on the scalar dissipation rate, which was also observed in [61]. Compare the two mechanisms, the shorter cool flame period and more intense low-temperature reaction in the rich zone, in combination with diffusion transport, could lead to earlier high-temperature ignition in the LLNL case, while retarded cool-flame ignition is exhibited as a consequence of the longer CFID at lean mixtures. This observation can also be applied to the remaining cases presented in Figure 10(b)-(c) and Figure 11(b)-(c), namely PRF40 and PRF80 at the baseline condition, as well as PRF0 at T_{amb} = 1000 K and O_2 = 21% ambient conditions, which is consistent with the previous discussion on homogeneous reactors. Unsurprisingly, it does not hold for the 800-K ambient condition presented in Figure 11(a), where the LLNL scheme predicts earlier cool-flame ignition, but this is in agreement with its shorter CFID as depicted in Figure 7(a). Stemming from these analyses, it could be concluded that the low-temperature chemistry, in particular the predictions of ignition and duration of the cool flame for different mixtures, is of crucial importance in determining the laminar flame structures, and more importantly, all the information of chemistry is still well-preserved at this operation step of the TFPV model.

To investigate how chemistry affects the auto-ignition process in turbulent spray flames, the apparent heat release rate computed from the two mechanisms are plotted in Figure 12, where the two-stage ignition for PRF0 and PRF40 at the baseline condition is represented. Regarding the first-stage ignition, which is primarily affected by the

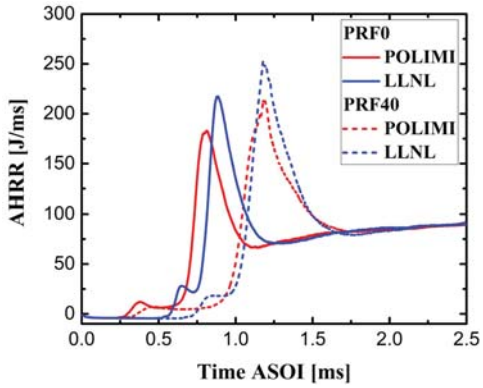

Figure 12: Computed apparent heat release rate for PRF0 and PRF40 at the baseline condition.

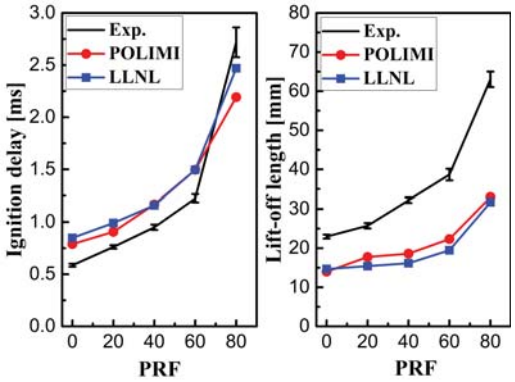

Figure 13: Comparison between measured and computed ignition delay and lift-off length as a function of PRF number.

low-temperature chemistry, the behaviors of the two mechanisms in reacting sprays are consistent with the ones in homogeneous reactors and laminar flames, where the POLIMI mechanism estimates a lower value of CFID, together with a longer duration of cool-flame period. However, the second-stage ignition also takes place earlier in the POLIMI cases, which is in contrast with the intrinsic chemistry characteristics of the two mechanisms as discussed in Figure 6 and Figure 10, where higher values of ID are computed by the POLIMI mechanism. This could be explained by the shortening of the cool-flame period due to the presence of high scalar dissipation rates in the turbulent spray flame, which accelerates the diffusion of progress variable, favoring the completeness of the cool-flame ignition in rich mixtures and promoting the high-temperature ignition to take place. This aspect highlights the fact that the description of low-temperature chemistry, especially the CFID prediction, is very relevant in determining the auto-ignition process in spray flames where the strong turbulent transport and diffusion is present.

To evaluate the performance of these two mechanisms, Figure 13 compares the measured and computed ID and LOL as a function of PRF number for the baseline condition. Following the suggestions from the ECN, ID is defined as the time from the start of injection to the time where the rising rate of maximum temperature reaches the highest value, while LOL is defined as the axial distance from the injector orifice to the first location where the OH mass fraction reaches 14% of its maximum value in the CFD domain. It is possible to see the TFPV model could correctly predict an increase of ID and LOL when augmenting PRF number, and the POLIMI mechanism computes lower ID times in compliance with the aforementioned

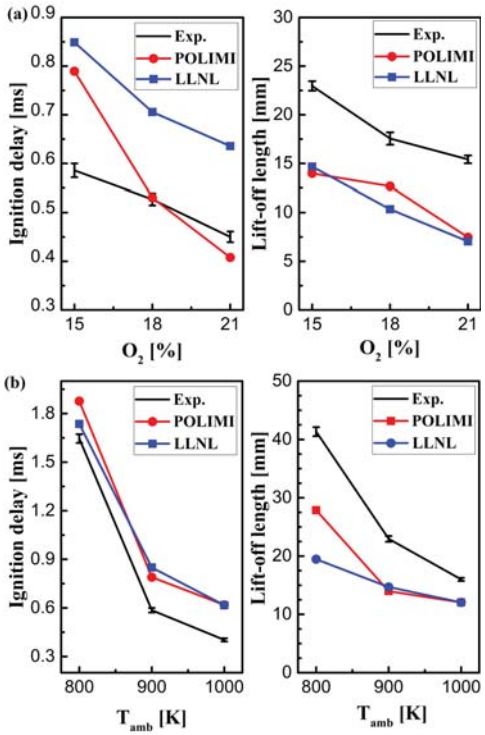

Figure 14: Comparison between measured and computed ignition delay and lift-off length for the parametric variations of (a) oxygen concentration and (b) ambient temperature.

considerations in Figure 12 and higher values of LOL, yielding a better agreement with experiments. This might be interpreted by the lower reactivity of rich mixtures, which requires a longer time to reach auto-ignition at the lift-off location. It is worth mentioning that the impact of chemistry on LOL prediction is lessened when flame stabilizes very close to the nozzle, where the local scalar dissipation rate exceeds the extinction value and the mixture fraction is too rich. At this point, it is possible to conclude that the chemistry information persists at all the stages of the TFPV operation, including the HR chemistry table and the TFPV table (laminar flames) generation, as well as the 3D reacting spray simulations. Figure 14 gathers the measured and computed LOL and ID for PRF0 at different oxygen concentration and ambient temperature conditions. Figure 14 (a) presents that the LLNL scheme overpredicts the ID in the oxygen sweep but providing a good parallelism with experimental data, and the sensitivity of LOL to oxygen concentration is well captured by both mechanisms. In Figure 14 (b), the computed ID from both mechanisms is in a good agreement with experiment data, and the POLIMI scheme predicts a higher value of LOL at 800-K ambient, being closer to the measurement. However, the underestimation of LOL is observed in all the cases, no matter using the POLIMI or LLNL mechanism. A possible reason for such discrepancy could be related to the diffusion of progress variable, linking with several factors, including the definition of progress variable and the description of turbulent diffusivity.

Optimization of turbulent Schmidt number

Bearing in mind that the turbulent Schmidt number Sc_t was applied to close the scalar-flux term in both mixture fraction and progress variable transport equations and with the intent to analyze how Sc_t affects each scalar, the investigation starts with the non-reacting modeling, followed by the reacting turbulent spray simulations

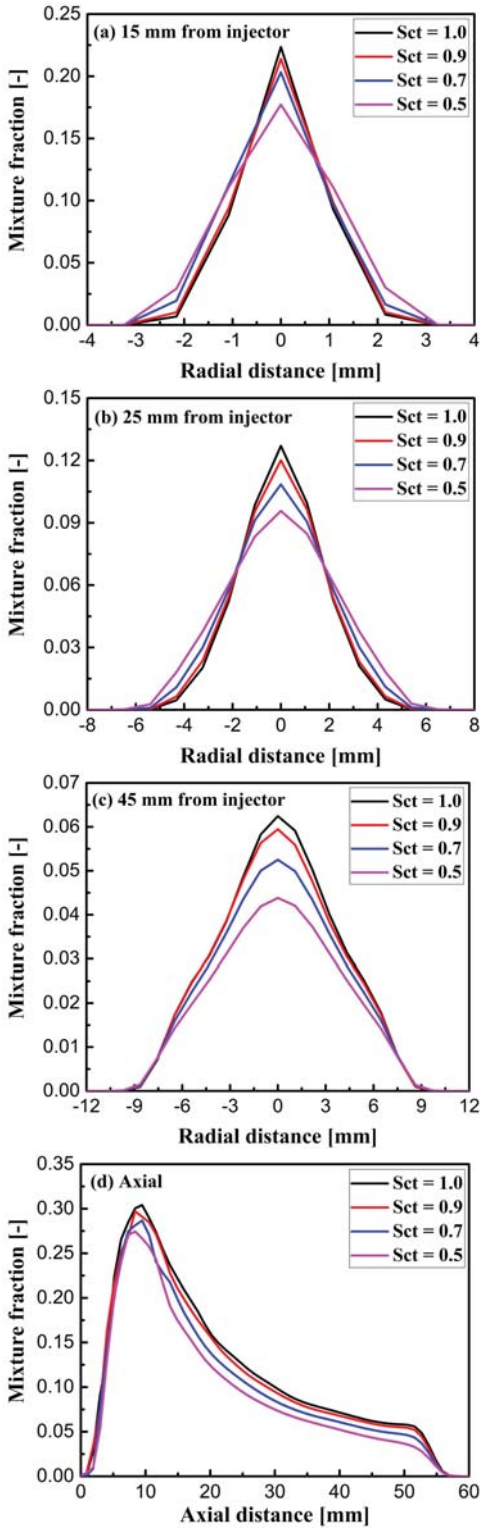

Figure 15: Comparison between radial mixture fraction distributions at (a) 15 mm, (b) 25 mm, (c) 45 mm from the injector and (d) axial mixture fraction distribution for different Sc_t values at 1.5 ms ASOI).

conducted using the POLIMI mechanism. Figure 15 presents the axial and radial $\widetilde{Z}$ distributions at 15 mm, 25mm, and 45 mm from the injector for the inert case under a steady condition (1.5 ms ASOI). The

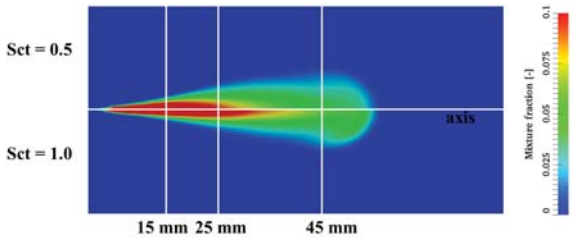

Figure 16: Mixture fraction distribution for Sc_t = 0.5 and Sc_t = 1.0 at 1.5 ms ASOI.

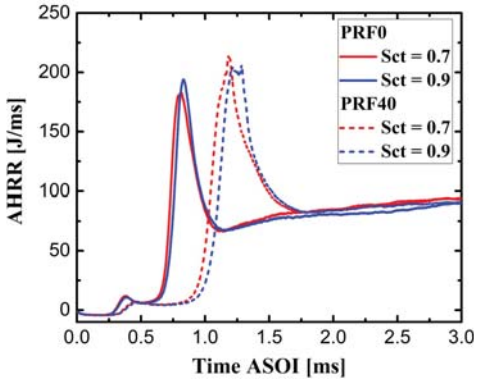

Figure 17: Comparison between apparent heat release rate for different Sc_t values.

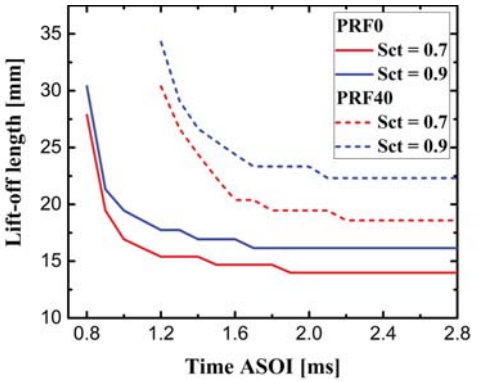

Figure 18: Comparison between lift-off length evolution for different Sc_t values.

choice of Sc_t is of paramount importance in describing the fuel-air mixing, and a lower value of Sc_t could smooth the distribution of mixture and reduce the peak values of Z on the axis due to the larger turbulence diffusivity, which also leads to a higher value of Z at longer radial distance for 15 mm and 25 mm axial locations. However, Z is reduced within the entire radial distribution range when moving further downstream to 45 mm from the injector. To better interpret this aspect, Figure 16 compares the mixture fraction distributions for Sc_t = 0.5 and Sc_t = 1.0 at 1.5 ms. It is possible to see that for Sc_t = 0.5, less fuel penetrates to the downstream region due to the larger radial dispersion, leading to the presence of leaner mixture in the entire spray tip. This might promote the formation of ignitable sites and subsequently anticipate the auto-ignition, as confirmed in Figure 17, which compares the apparent heat release rate for Sc_t = 0.7 and Sc_t = 0.9 and depicts the lower value provides slightly shorter ID time for both PRF0 and PRF40 at the baseline condition. In Figure 18,

effects of Sc_t on the time evolution of LOL are presented for PRF0 and PRF40, evidencing flame stabilized further upstream in the case of Sc_t = 0.7. This might be attributed to two factors: (1) the facilitated diffusion of mixture fraction moves the auto-ignition location, represented by the first appearance of LOL, further upstream; (2) the enhanced diffusion of progress variable imposes the chemical reactivity and promotes the auto-ignition of upstream mixtures.

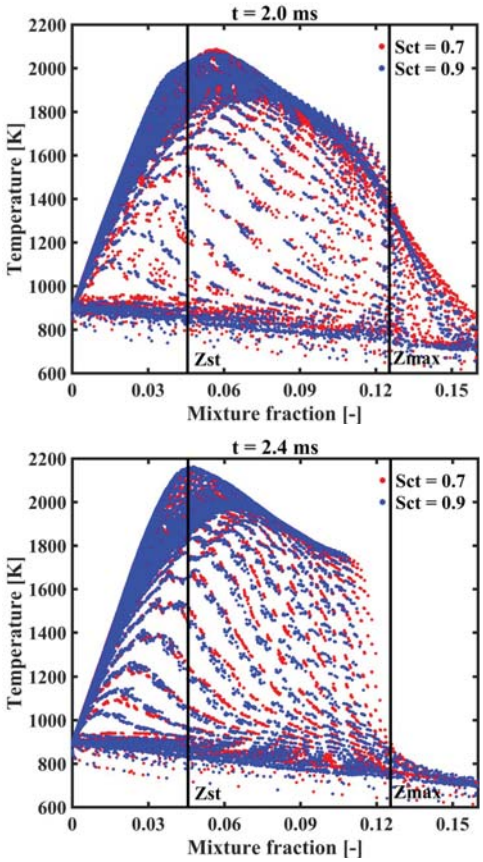

Figure 19: Scatter plots of temperature as a function of mixture fraction for (a) PRF0 and (b) PRF40 under steady conditions. Mixture fractions corresponding to $\phi = 1$ and $\phi = 3$ are shown in black solid lines and labeled as Z_{st} and Z_{max}, respectively.

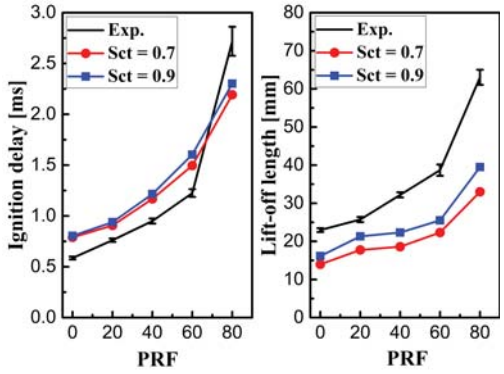

Figure 20: Comparison between the measured and computed ignition delay and lift-off length as a function of PRF number.

To substantiate the second consideration, Figure 19 presents the scatter plots of temperature, a representative of progress variable, as a

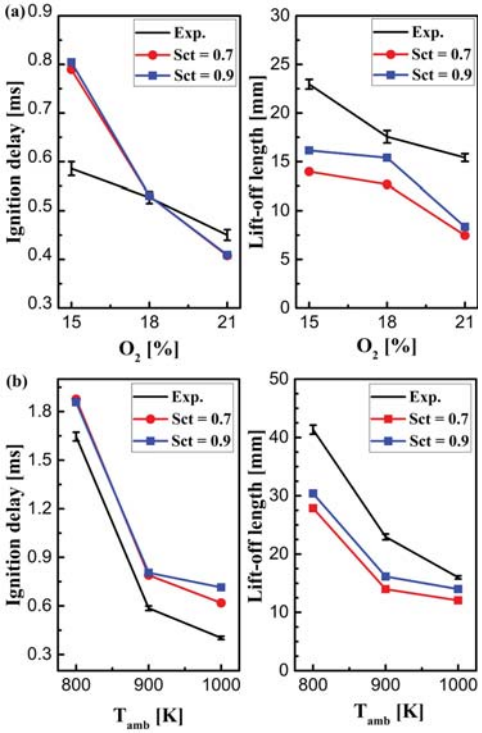

Figure 21: Comparison between the measured and computed ignition delay and lift-off length for the parametric variations of (a) oxygen concentration and (b) ambient temperature.

function of mixture fraction for PRF0 and PRF40 under steady conditions, with Z_{st} and Z_{max} depicted by black solid lines. It is possible to see the rich flammability limit is slightly extended in the case of Sc_t = 0.7 due to the higher progress variable diffusion, causing the flame stabilization more upstream. Such impact is alleviated when flame stabilizes at rich mixtures ($Z > Z_{max}$) where the reaction rate is set to zero, as illustrated in Figure 19 (a). This also explains why the PRF0 case exhibits less sensitivity to Sc_t in Figure 17 (b).

To find the optimum value of Sc_t, in Figure 20, the computed and measured ID and LOL are compared as a function of PRF number. In line with the preceding discussion, lower values of ID and LOL are predicted with Sc_t = 0.7, showing a satisfactory accuracy of ID prediction, but an underestimation of LOL. Increasing Sc_t to 0.9 can improve the prediction of LOL, and more importantly, with negligible deterioration of ID prediction. The same observations can be made for the remaining cases, as presented in Figure 21, considering the parametric variations of ambient temperature and oxygen concentration for PRF0. Further increasing the value of Sc_t was not conducted, since it is well established in the literature that the diffusion of mass or energy is greater than that of momentum. As a final remark, the authors are aware of that applying a constant Sc_t across the whole flow field, irrespective of the turbulence structure, has been questioned by experimental and DNS observations, especially in combustion systems [66, 67, 68, 34]. To this end, calculating Sc_t as a solution of the turbulence model [35, 67, 31] will be one of the interesting future investigations in reacting sprays.

Validation and evaluation of the TFPV model

To comprehensively validate the TFPV model, the parametric variations of oxygen concentration and ambient temperature were performed in the fuel content sweep, and the comparison between

measured and computed LOL and ID is presented in Figure 22. Results for O2 = 18% and O_2 = 21% are plotted in Figure 22 as a function of PRF number, evidencing that satisfactory predictions of ID and LOL are achieved by the TFPV model from PRF0 and PRF60, while an underestimation of ID and the consequent low value of LOL is observed in the case of PRF80. This might be attributed to the choice of chemical mechanism, most likely, it is too reactive for PRF80 under rich oxygen conditions.

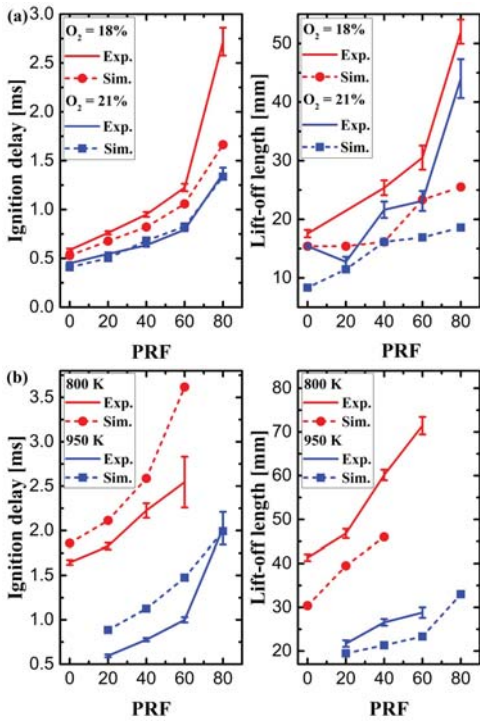

Figure 22: Comparison between the measured and computed ignition delay and lift-off length as a function of PRF number for (a) O_2 = 18% and O_2 = 21% conditions and (b) T_{amb} = 800 K and T_{amb} = 950 K conditions.

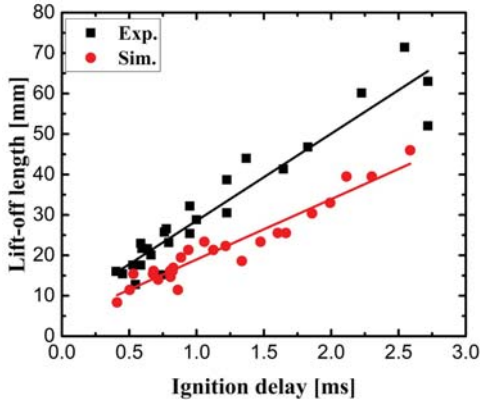

Figure 23: Correlation between ignition delay and lift-off length for experiments and simulations.

In Figure 22 (b), two ambient temperature, T_{amb} = 800 K and T_{amb} = 950 K are considered for all the fuels. An increase of ID and LOL with PRF number is correctly captured by the TFPV model at both ambient temperatures. Computed ID times are longer than the measured ones, but such discrepancy might be more related to the description of mixing and chemistry, instead of the combustion model. For this reason, authors will go back to the non-reacting calculations, and perform a more detailed investigation on the turbulence and spray model constants in the future work. An underestimation of LOL is also observed, and this is more evidently illustrated in Figure 23, where the correlation between ID and LOL are compared for experiments and simulations. As can be seen, the computed slope is smaller than the measured one, indicating probably the TFPV model is not fully capable to provide a very accurate estimation of LOL. This might be explained by the steep gradient of progress variable from the ignition sites, which generates very intense diffusion flux, transporting the progress variable upstream. This could accelerate the ignition of rich mixtures in the upstream and lead to a fast flame stabilization. Probably changing its definition could provide a better trajectory of the progress variable, which may potentially overcome this limitation and improve the results. More efforts will be dedicated to this aspect.

Conclusion

The main objective of this study is to extensively assess the potentialities and limits of the tabulated flamelet progress variable (TFPV) approach for modeling turbulent Diesel sprays with primary reference fuels (PRFs). In particular, n-heptane, iso-octane, and four intermediate blends were tested, representing the transition from conventional Diesel fuel to a gasoline-like one in terms of ignition behavior. Simulations were initially carried out across a wide range operating conditions to assess the performance of two kinetic mechanisms and the choice of turbulent Schmidt number Sc_t. The parametric variations of ambient temperature and oxygen concentration were then performed for each fuel to comprehensively validate the TFPV model. Key findings in this work can be briefly summarized as follows:

- The chemistry information was persisted in all the computational steps of the TFPV model, including the homogeneous chemistry table generation, the unsteady diffusion flame calculations, and the turbulent spray flame simulations, proving its capability to capture subtle differences between chemical mechanisms. Besides, a reaction path analysis might be necessary to better explain the different performance between these two chemistry mechanisms in Diesel spray flames simulations, which is of great interest for future investigation;
- The low-temperature chemistry, in particular the description of the start and duration of cool flames for different mixtures, was of crucial importance in determining the laminar flame structures. Regarding the reacting sprays, the presence of high scalar dissipation rate could accelerate the diffusion of progress variable produced from the cool flame, facilitating the completion of the cool flame period and the start of high-temperature ignition, which further underlines the key role of low-temperature chemistry;
- The use of Sc_t = 0.9 showed a superior performance to Sc_t = 0.7, yielding a better agreement with experimental data in terms of LOL due to the reduced turbulent diffusivity. It was observed that the lower Sc_t could enhance the mixture fraction diffusion, causing the ignition to take place earlier and more upstream, and also promote the progress variable diffusion, imposing the chemical reactivity of upstream mixtures and favoring the auto-ignition in this region, which consequently reduces the LOL;
- An increase of ID and LOL with PRF number was well-captured by the TFPV model, demonstrating its validity in both diffusion and partial-premixed combustion modes. However, not to be ignored, the slope between LOL and ID was underestimated by the TFPV model and the analysis indicated that using a more appropriate definition of progress variable could have the potential to improve the accuracy, which will be surely investigated in the future work.

References

1. M. Badami, F. Mallamo, F. Millo, and E. E. Rossi, "Influence of Multiple Injection Strategies on Emissions, Combustion Noise and BSFC of a DI Common Rail Diesel Engine," *SAE Transactions*, vol. 111, pp. 1118–1129, 2002, doi:10.4271/2002-01-0503.
2. F. Zhao, T. N. Asmus, D. N. Assanis, J. E. Dec, J. A. Eng, and P. M. Najt, "Homogeneous Charge Compression Ignition (HCCI) Engines," SAE Technical Paper PT-94, 2003.
3. M. Y. E. Selim, "Sensitivity of dual fuel engine combustion and knocking limits to gaseous fuel composition," *Energy Conversion and Management*, vol. 45, pp. 411–425, 2004, doi:10.1016/S0196-8904(03)00150-X.
4. R. D. Reitz and G. Duraisamy, "Review of high efficiency and clean reactivity controlled compression ignition (RCCI) combustion in internal combustion engines," *Progress in Energy and Combustion Science*, vol. 46, pp. 12–71, 2015, doi:10.1016/j.pecs.2014.05.003.
5. G. T. Kalghatgi, "The outlook for fuels for internal combustion engines," *International Journal of Engine Research*, vol. 15, pp. 383–398, 2014, doi:10.1177/1468087414526189.
6. X. Lu, D. Han, and Z. Huang, "Fuel design and management for the control of advanced compression-ignition combustion modes," *Progress in Energy and Combustion Science*, vol. 37, pp. 741–783, 2011, doi:10.1016/j.pecs.2011.03.003.
7. J. J. Lopez, J. M. Garcia-Oliver, A. Garcia, and V. Domenech, "Gasoline effects on spray characteristics, mixing and auto-ignition processes in a CI engine under Partially Premixed Combustion conditions," *Applied Thermal Engineering*, vol. 70, pp. 996–1006, 2014, doi:10.1016/j.applthermaleng.2014.06.027.
8. R. Payri, J. M. Garcia-Oliver, T. Xuan, and M. Bardi, "A study on diesel spray tip penetration and radial expansion under reacting conditions," *Applied Thermal Engineering*, vol. 90, pp. 619–629, 2015, doi:10.1016/j.applthermaleng.2014.06.027.
9. T. I. Farouk, Y. Xu, C. T. Avedisian, and F. L. Dryer, "Combustion characteristics of primary reference fuel (PRF) droplets: Single stage high temperature combustion to multistage Cool Flame behavior," *Proceedings of the Combustion Institute*, vol. 36, pp. 2585–2594, 2017, doi:10.1016/j.proci.2016.07.066.
10. S. Bhattachar.jee and D. C. Haworth, "Simulations of transient n-heptane and n-dodecane spray flames under engine-relevant conditions using a transported PDF method," *Combustion and Flame*, vol. 160, pp. 2083–2102, 2013, doi:10.1016/j.combustflame.2013.05.003.
11. V. Mittal, D. J. Cook, and H. Pitsch, "An extended multi-regime flamelet model for IC engines," *Combustion and Flame*, vol. 159, pp. 2767–2776, 2012, doi:10.1016/j.combustflame.2012.01.014.
12. S.-C. Kong, Z. Han, and R. D. Reitz, "The Development and Application of a Diesel Ignition and Combustion Model for Multidimensional Engine Simulation," *SAE Transactions*, vol. 104, pp. 502–518, 1995, doi:10.4271/950278.
13. O. Colin and A. Benkenida, "The 3-zones extended coherent flame model (ECFM3z) for computing premixed/diffusion combustion," *Oil & Gas Science and Technology*, vol. 59, pp. 593–609, 2004, doi:10.2516/ogst:2004043.
14. D. C. Haworth, "Progress in probability density function methods for turbulent reacting flows," *Progress in Energy and Combustion Science*, vol. 36, pp. 168–259, 2010, doi:10.1016/j.pecs.2009.09.003.
15. A. Felden, L. Esclapez, E. Riber, B. Cuenot, and H. Wang, "Including real fuel chemistry in LES of turbulent spray combustion," *Combustion and Flame*, vol. 193, pp. 397–416, 2018, doi:10.1016/j.combustflame.2018.03.027.
16. J. A. van Oijen, F. A. Lammers, and L. P. H. de Goey, "Modeling of complex premixed burner systems by using flamelet-generated manifolds," *Combustion and Flame*, vol. 127, pp. 2124–2134, 2001, doi:10.1016/S0010-2180(01)00316-9.
17. O. Gicquel, N. Darabiha, and D. Thevenin, "Liminar premixed hydrogen/air counterflow flame simulations using flame prolongation of ILDM with differential diffusion," *Proceedings of the Combustion Institute*, vol. 28, pp. 1901–1908, 2000, doi:10.1016/S0082-0784(00)80594-9.
18. C. D. Pierce and P. Moin, "Progress-variable approach for large-eddy simulation of non-premixed turbulent combustion," *Journal of Fluid Mechanics*, vol. 504, pp. 73–97, 2004, doi:10.1017/S0022112004008213.
19. M. Lionel, M. Jean-Baptiste, J. Stephane, and C. Olivier, "Evaluation of different tabulation techniques dedicated to the prediction of the combustion and pollutants emissions on a diesel engine with 3d cfd," SAE Technical Paper 2013-01-1093, 2015, doi:10.4271/2013-01-1093.
20. B. Naud, R. Novella, J. M. Pastor, and J. F. Winklinger, "RANS modelling of a lifted H2/N2 flame using an unsteady flamelet progress variable approach with presumed PDF," *Combustion and Flame*, vol. 162, pp. 893–906, 2015, doi:10.1016/j.combustflame.2014.09.014.
21. J.-B. Michel, O. Colin, C. Angelberger, and D. Veynante, "Using the tabulated diffusion flamelet model ADF-PCM to simulate a lifted methane air jet flame," *Combustion and Flame*, vol. 156, pp. 1318–1331, 2009, doi:10.1016/j.combustflame.2008.12.012.
22. T. Lucchini, D. Pontoni, G. D'Errico, and B. Somers, "Modeling diesel combustion with tabulated kinetics and different flame structure assumptions based on flamelet approach," *International Journal of Engine Research*, vol. 21, pp. 89–100, 2020, doi:10.1177/1468087419862945.
23. Q. Zhou, T. Lucchini, G. D'Errico, N. Maes, B. Somers, and X.-c. Lu, "Computational Modeling of Diesel Spray Combustion with Multiple Injections," SAE Technical Paper 2020-04-25, 2020, doi:10.4271/2020-01-1155.
24. T. Lucchini, G. D'Errico, T. Cerri, A. Onorati, and G. Hardy, "Experimental validation of combustion models for diesel engines based on tabulated kinetics in a wide range of operating conditions," SAE Technical Paper 2017-01-15, 2017, doi:10.4271/2017-24-0029.
25. Q. Zhou, T. Lucchini, G. D'Errico, and G. Hardy, "Validation of Diesel combustion models with turbulence chemistry interaction and detailed kinetics," SAE Technical Paper 2019-24-0088, 2019, doi:10.4271/2019-24-0088.
26. M. Jangi, T. Lucchini, C. Gong, and X.-S. Bai, "Effects of fuel cetane number on the structure of diesel spray combustion: An accelerated Eulerian stochastic fields method," *Combustion Theory and Modelling*, vol. 19, pp. 549–567, 2015, doi:10.1080/13647830.2015.1057234.
27. I. Yimer, I. Campbell, and L.-Y. Jiang, "Estimation of the Turbulent Schmidt Number from Experimental Profiles of Axial Velocity and Concentration for High-Reynolds-Number Jet Flows," *Canadian Aeronautics and Space Journal*, vol. 48, pp. 195–200, 2002, doi:10.5589/q02-024.
28. D. B. Spalding, "Concentration fluctuations in a round turbulent free jet," *Chemical Engineering Science*, vol. 26, pp. 95–107, 1971, doi:10.1016/0009-2509(71)86083-9.
29. B. E. Launder, "Heat and Mass Transport," in *Turbulence* (P. Bradshaw, ed.), Topics in Applied Physics, pp. 231–287, Berlin, Heidelberg: Springer, 1976.

30. Y. Tominaga and T. Stathopoulos, "Turbulent Schmidt numbers for CFD analysis with various types of flowfield," *Atmospheric Environment*, vol. 41, pp. 8091–8099, 2007, doi:10.1016/j.atmosenv.2007.06.054.

31. D. P. Combest, P. A. Ramachandran, and M. P. Dudukovic, "On the Gradient Diffusion Hypothesis and Passive Scalar Transport in Turbulent Flows," *Industrial & Engineering Chemistry Research*, vol. 50, pp. 8817–8823, 2011, doi:10.1021/ie200055s.

32. G. Mompean, "Three-equation turbulence model for prediction of the mean square temperature variance in grid-generated flows and round jets," *International Journal of Heat and Mass Transfer*, vol. 37, pp. 1165–1172, 1994, doi:10.1016/0017-9310(94)90202-X.

33. D. S. Crocker, D. Nickolaus, and C. E. Smith, "CFD Modeling of a Gas Turbine Combustor From Compressor Exit to Turbine Inlet," *Journal of Engineering for Gas Turbines and Power*, vol. 121, pp. 89–95, 1999, doi:10.1115/1.2816318.

34. D. Eklund, R. Baurle, and M. Gruber, "Numerical study of a scramjet combustor fueled by an aerodynamic ramp injector in dual-mode combustion," in *39th Aerospace Sciences Meeting and Exhibit*, American Institute of Aeronautics and Astronautics.

35. X. Xiao, J. R. Edwards, H. A. Hassan, and A. D. Culter, "Variable Turbulent Schmidt-Number Formulation for Scramjet Applications," *AIAA J*, vol. 44, no. 3, pp. 593–599, 2006, doi:10.2514/1.15450.

36. Engine Combustion Network, https://ecn.sandia.gov

37. J. M. Desantes, J. M. Garcia-Oliver, T. Xuan, and W. Vera-Tudela, "A study on tip penetration velocity and radial expansion of reacting diesel sprays with different fuels," *Fuel*, vol. 207, pp. 323–335, 2017, doi:10.1016/j.fuel.2017.06.108.

38. J. V. Pastor, J. M. Garcia-Oliver, J. J. Lopez, and W. Vera-Tudela, "An experimental study of the effects of fuel properties on reactive spray evolution using Primary Reference Fuels," *Fuel*, vol. 163, pp. 260–270, 2016, doi:10.1016/j.fuel.2015.09.064.

39. T. Lucchini, G. D'Errico, A. Onorati, A. Frassoldati, A. Stagni, and G. Hardy, "Modeling Non-Premixed Combustion Using Tabulated Kinetics and Different Fame Structure Assumptions," *SAE International Journal of Engines*, vol. 10, no. 2, pp. 593–607, 2017, doi:10.4271/2017-01-0556.

40. G. D'Errico, T. Lucchini, A. Onorati, and G. Hardy, "Computational fluid dynamics modeling of combustion in heavy-duty diesel engines," *International Journal of Engine Research*, vol. 16, pp. 112–124, 2015, doi:10.1177/1468087414561276.

41. H. Lehtiniemi, Y. Zhang, R. Rawat, and F. Mauss, "Efficient 3-D CFD Combustion Modeling with Transient Flamelet Models," SAE Technical Paper 2008-01-0957, 2008, doi:10.4271/2008-01-0957.

42. H. Barths, C. Hasse, and N. Peters, "Computational fluid dynamics modelling of non-premixed combustion in direct injection diesel engines," *International Journal of Engine Research*, vol. 1, pp. 249–267, 2000, doi:10.1243/1468087001545164.

43. N. Peters, "Laminar diffusion flamelet models in non-premixed turbulent combustion," *Progress in Energy and Combustion Science*, vol. 10, pp. 319–339, 1984, doi:10.1016/0360-1285(84)90114-X.

44. G. D'Errico, T. Lucchini, R. Di Gioia, and G. Bonandrini, "Application of the CTC Model to Predict Combustion and Pollutant Emissions in a Common-Rail Diesel Engine Operating with Multiple Injections and High EGR," SAE Technical Paper 2012-01-0154, 2012, doi:10.4271/2012-01-0154.

45. T. Lucchini, L. Cornolti, G. Montenegro, G. D'Errico, M. Fiocco, A. Teraji, and T. Shiraishi, "A Comprehensive Model to Predict the Initial Stage of Combustion in SI Engines," SAE Technical Paper 2013-01-1087, 2013, doi:10.4271/2013-01-1087.

46. T. Lucchini, A. Della Torre, G. D'Errico, G. Montenegro, M. Fiocco, and A. Maghbouli, "Automatic Mesh Generation for CFD Simulations of Direct-Injection Engines," SAE Technical Paper 2015-01-0376, 2015, doi:10.4271/2015-01-0376.

47. S. B. POPE, "An explanation of the turbulent round-jet/plane-jet anomaly," *AIAA Journal*, vol. 16, no. 3, pp. 279–281, 1978, doi:10.2514/3.7521.

48. J. H. Ferziger and M. Peric, *Computational Methods for Fluid Dynamics*. Springer Science & Business Media, 2012.

49. R. Reitz, "Modeling atomization processes in high-pressure vaporizing sprays," *Atomisation Spray Technology*, vol. 3, pp. 309–337, Jan. 1987.

50. R. D. Reitz and R. Diwakar, "Effect of Drop Breakup on Fuel Sprays," SAE Technical Paper 860469, 1986, doi:10.4271/860469.

51. C. Baumgarten, *Mixture Formation in Internal Combustion Engines*. Heat and Mass Transfer, Berlin Heidelberg: Springer-Verlag, 2006.

52. T. Lucchini, G. D'Errico, and D. Ettorre, "Numerical investigation of the spray-mesh-turbulence interactions for high-pressure, evaporating sprays at engine conditions," *International Journal of Heat and Fluid Flow*, vol. 32, pp. 285–297, 2011, doi:10.1016/j.ijheatfluidflow.2010.07.006.

53. Q. Zhou, T. Lucchini, G. D'Errico, G. Hardy, and X. Lu, "Modeling heavy-duty diesel engines using tabulated kinetics in a wide range of operating conditions," *International Journal of Engine Research*, p. 1468087419896165, 2020, doi:10.1177/1468087419896165.

54. E. Ranzi, A. Frassoldati, A. Stagni, M. Pelucchi, A. Cuoci, and T. Faravelli, "Reduced Kinetic Schemes of Complex Reaction Systems: Fossil and Biomass-Derived Transportation Fuels," *International Journal of Chemical Kinetics*, vol. 46, no. 9, pp. 512–542, 2014, doi:10.1002/kin.20867.

55. A. Stagni, A. Cuoci, A. Frassoldati, T. Faravelli, and E. Ranzi, "Lumping and Reduction of Detailed Kinetic Schemes: an Effective Coupling," *Industrial & Engineering Chemistry Research*, vol. 53, pp. 9004–9016, 2014, doi:10.1021/ie403272f.

56. A. Stagni, A. Frassoldati, A. Cuoci, T. Faravelli, and E. Ranzi, "Skeletal mechanism reduction through species-targeted sensitivity analysis," *Combustion and Flame*, vol. 163, pp. 382–393, 2016, doi:10.1016/j.combustflame.2015.10.013.

57. M. Mehl, W. J. Pitz, C. K. Westbrook, and H. J. Curran, "Kinetic modeling of gasoline surrogate components and mixtures under engine conditions," *Proceedings of the Combustion Institute*, vol. 33, pp. 193–200, 2011, doi:10.1016/j.proci.2010.05.027.

58. R. Payri, J. M. Garcia-Oliver, M. Bardi, and J. Manin, "Fuel temperature influence on diesel sprays in inert and reacting conditions," *Applied Thermal Engineering*, vol. 35, pp. 185–195, 2012, doi:10.1016/j.applthermaleng.2011.10.027.

59. D. Paredi, T. Lucchini, G. D'Errico, A. Onorati, L. Pickett, and J. Lacey, "CFD modeling of spray evolution for spark-ignition, direct injection engines," *AIP Conference Proceedings*, vol. 2191, p. 020125, 2019, doi:10.1063/1.5138858.

60. D. Paredi, T. Lucchini, G. D'Errico, A. Onorati, L. Pickett, and J. Lacey, "Validation of a comprehensive computational fluid dynamics methodology to predict the direct injection process of gasoline sprays using Spray G experimental data," *International*

Journal of Engine Research, vol. 21, pp. 199–216, 2020, doi:10.1177/1468087419868020.

61. F. Payri, J. M. Garcia-Oliver, R. Novella, and E. J. Perez-Sanchez, "Influence of the n-dodecane chemical mechanism on the CFD modelling of the diesel-like ECN Spray A flame structure at different ambient conditions," *Combustion and Flame*, vol. 208, pp. 198–218, 2019, doi:10.1016/j.combustflame.2019.06.032.
62. E. Mastorakos, "Ignition of turbulent non-premixed flames," *Progress in Energy and Combustion Science*, vol. 35, pp. 57–97, 2009, doi:10.1016/j.pecs.2008.07.002.
63. E. Mastorakos, T. A. Baritaud, and T. J. Poinsot, "Numerical simulations of autoignition in turbulent mixing flows," *Combustion and Flame*, vol. 109, pp. 198–223, 1997, doi:10.1016/S0010-2180(96)00149-6.
64. R. N. Dahms, G. A. Paczko, S. A. Skeen, and L. M. Pickett, "Understanding the ignition mechanism of high-pressure spray flames," *Proceedings of the Combustion Institute*, vol. 36, pp. 2615–2623, 2017, doi:10.1016/j.proci.2016.08.023.
65. C. Gong, M. Jangi, and X.-S. Bai, "Large eddy simulation of n-Dodecane spray combustion in a high pressure combustion vessel," *Applied Energy*, vol. 136, pp. 373–381, 2014, doi:10.1016/j.apenergy.2014.09.030.
66. S. Nishiki, T. Hasegawa, R. Borghi, and R. Himeno, "Modelling of turbulent scalar flux in turbulent premixed flames based on DNS databases," *Combustion Theory and Modelling*, vol. 10, pp. 39–55, 2006, doi:10.1080/13647830500307477.
67. P. Keistler, X. Xiao, H. Hassan, and C. Rodriguez, "Simulation of Supersonic Combustion Using Variable Turbulent Prandtl/Schmidt Number Formulation," in *36th AIAA Fluid Dynamics Conference and Exhibit*, doi:10.2514/6.2006-3733.
68. T. Watanabe, Y. Sakai, K. Nagata, and O. Terashima, "Turbulent Schmidt number and eddy diffusivity change with a chemical reaction," *Journal of Fluid Mechanics*, vol. 754, pp. 98–121, 2014, doi:10.1017/jfm.2014.387.

Contact Information

Qiyan Zhou, Ph.D.
Department of Energy, Politecnico di Milano
Via Lambruschini, 4
20156 Milano, Italy
qiyan.zhou@polimi.it

Acknowledgments

Authors acknowledge the financial support from the China Scholarship Council (No. 201806230180) and Natural Science Foundation of China (No. 51961135105) for the first author's study in Politecnico di Milano, Italy